

NUMERICAL INVESTIGATION OF TWO-DIMENSIONAL FLOWS OF NEMATIC LIQUID CRYSTALS

Pedro A. Cruz, pedroac@icmc.usp.br

Murilo F. Tomé, murilo@icmc.usp.br

Universidade de São Paulo - São Carlos - Brasil

Iain W. Stewart, iws@maths.strath.ac.uk

Sean McKee, smck@maths.strath.ac.uk

University of Strathclyde - Glasgow - Scotland

Abstract. We present a numerical method for solving two-dimensional nematic liquid crystal flows subject to a magnetic field. The dynamic equations of nematic liquid crystals are based on the Ericksen-Leslie dynamic theory. This theory accounts for fluid anisotropy and elastic stresses resulting from spatial distortion of the “director”, which is a vector field describing the local average molecular orientation. A numerical method for solving the governing equations for 2D flows has been formulated. The basic equations are solved by a finite difference technique based on the GENSMAC methodology introduced by Tomé and McKee (1994), Tomé et al. (2002). Channel flow was simulated and by using mesh refinement validated results are given. To demonstrate the capabilities of the numerical method, the flow of a nematic liquid crystal through a two-dimensional L-shaped channel was simulated. Results are presented for several values of the Reynolds and Ericksen numbers.

Keywords: Two-dimensional flow, Ericksen-Leslie equations, Nematic liquid crystals, Magnetic field, Finite difference

1. INTRODUCTION

The basic theory that describes the dynamics of nematic liquid crystals is the “Ericksen-Leslie dynamic theory”, proposed by Ericksen (1961), Leslie (1966), Leslie (1968) in the sixties. This theory has consistently been applied to many flow problems of nematic liquid crystals, but the equations are complex so that analytic solutions of nematic liquid crystals flows are extremely rare. Consequently, numerical methods are becoming an important tool for solving the highly nonlinear equations governing the flow of nematic liquid crystals.

In the literature there are many articles treating the flow of nematic liquid crystals (see for example Pieranski and Guyon (1974), Pikin (1974), Jenkins (1978), Heuer, Knepe and Schneider (1991), Chono and Tsuji (1998), Chono, Tsuji and Denn (1998), Baleo, Vincent and Navard (1998)). For instance, Pikin (1974) formulated a one-dimensional model to study the influence of shear forces on the orientation of a nematic liquid crystal and obtained some approximate solutions for the Ericksen-Leslie equations while MacSithigh and Currie (1977) considered strong shear flows and presented approximate solutions for the director orientation. In other studies, for example Pieranski and Guyon (1974), the investigation was through experimentation. Many issues in nematic liquid crystal flows have been investigated by solving the Ericksen-Leslie equations numerically. For instance, Baleo, Vincent and Navard (1998) neglected elasticity, in which case the equations reduce to the Ericksen TIF “Transversely Isotropic Fluids”. Chono, Tsuji and Denn (1998) studied the spatial development of the director orientation in tumbling nematic liquid crystals in channel flow. Chono and Tsuji (1998) analyzed the flow around a circular cylinder. However, to our knowledge, studies using the full Ericksen-Leslie equations for two-dimensional flows are extremely few and far between.

In this paper we present a finite difference technique for solving the full Ericksen-Leslie dynamic equations in two dimensions under the influence of a finite magnetic field. More specifically, we solve the Ericksen-Leslie dynamic equations in 2D and L-shaped channels and give steady state solutions for the director and velocity fields for various values of the Ericksen and Reynolds numbers.

2. THE ERICKSEN-LESLIE EQUATIONS

The Ericksen-Leslie dynamic equations for nematics in the incompressible isothermal case when the director inertial term is neglected can be stated concisely as follows, using the usual Einstein summation convention where appropriate. These are the most frequently used forms of the equations and we state them in the commonly accepted notation (see Stewart (2004)). They consist of the constraints

$$n_i n_i = 1, \quad u_{i,i} = 0, \quad (1)$$

together with the balance laws which arise from linear and angular momentum, namely,

$$\rho \dot{u}_i = -(p + w_F)_{,i} + \tilde{g}_j n_{j,i} + G_j n_{j,i} + \tilde{t}_{ij,j}, \quad (2)$$

$$\left(\frac{\partial w_F}{\partial n_{i,j}} \right)_{,j} - \frac{\partial w_F}{\partial n_i} + \tilde{g}_i + G_i = \lambda n_i, \quad (3)$$

where ρ is the density, G_i is the generalised body force (which is related to the external body moment K_i per unit mass through the relation $\rho K_i = \varepsilon_{ijk} n_j G_k$, p is the pressure, and w_F is the elastic energy density for nematics. In the one-constant approximation for the elastic constants, the elastic energy can be written as (see Stewart (2004))

$$w_F = \frac{1}{2} K \|n_{i,j}\|^2 = \frac{1}{2} K n_{i,j} n_{i,j}, \quad (4)$$

where $K > 0$ is an elastic constant. A comma indicates partial differentiation with respect to the variable it precedes; for example $n_{i,j}$ denotes the partial derivative of the i^{th} component of n_i with respect to the j^{th} variable. The usual material time derivative is denoted by a superposed dot. The scalar function λ is a Lagrange multiplier which can usually be eliminated or evaluated by taking the scalar product of Eq. (3) with n_i ; it arises from the constraint that n_i is a unit vector. The constitutive equations for the viscous stress \tilde{t}_{ij} and the vector \tilde{g}_i are

$$\tilde{t}_{ij} = \alpha_1 n_k A_{kp} n_p n_i n_j + \alpha_2 N_i n_j + \alpha_3 n_i N_j + \alpha_4 A_{ij} + \alpha_5 n_j A_{ik} n_k + \alpha_6 n_i A_{jk} n_k, \quad (5)$$

$$\tilde{g}_i = -\gamma_1 N_i - \gamma_2 A_{ip} n_p, \quad (6)$$

$$\gamma_1 = \alpha_3 - \alpha_2 \geq 0, \quad \gamma_2 = \alpha_3 + \alpha_2 = \alpha_6 - \alpha_5, \quad (7)$$

$$A_{ij} = \frac{1}{2}(u_{i,j} + u_{j,i}), \quad N_i = \dot{n}_i - W_{ij} n_j, \quad W_{ij} = \frac{1}{2}(u_{i,j} - u_{j,i}), \quad (8)$$

where $\alpha_1, \alpha_2, \dots, \alpha_6$, are the Leslie viscosities, A_{ij} is the rate of strain tensor, W_{ij} is the vorticity tensor, N_i is the rotational time flux of the director n_i and a superposed dot again represents the material time derivative. The coefficient γ_1 is often referred to as the twist or rotational viscosity and γ_2 is called the torsion coefficient. The viscous stress \tilde{t}_{ij} is in general asymmetric. The Parodi relation (see Parodi (1970))

$$\gamma_2 = \alpha_6 - \alpha_5 = \alpha_2 + \alpha_3, \quad (9)$$

is assumed to hold and the Leslie viscosities must additionally satisfy the inequalities (see Stewart (2004)):

$$\gamma_1 = \alpha_3 - \alpha_2 \geq 0, \quad \alpha_4 \geq 0, \quad 2\alpha_4 + \alpha_5 + \alpha_6 \geq 0, \quad (10)$$

$$2\alpha_1 + 3\alpha_4 + 2\alpha_5 + 2\alpha_6 \geq 0, \quad 4\gamma_1(2\alpha_4 + \alpha_5 + \alpha_6) \geq (\alpha_2 + \alpha_3 + \gamma_2)^2. \quad (11)$$

The stress tensor for nematic liquid crystals is given by

$$t_{ij} = -p \delta_{ij} - K n_{p,j} n_{p,i} + \tilde{t}_{ij}. \quad (12)$$

3. GOVERNING EQUATIONS

We consider the case of two-dimensional flow of a nematic liquid crystal. A magnetic field is applied and we assume the one-constant approximation for the elastic constants. The unitary director n_i and velocity v_i can be written in the general forms

$$\mathbf{n} = (\cos \phi, \sin \phi, 0), \quad \phi = \phi(x, y, t), \quad \mathbf{u} = (u(x, y, t), v(x, y, t), 0), \quad (13)$$

where ϕ is often referred to as the orientation angle of the director.

The magnetic field potential (equal to the negative of the magnetic energy) is

$$\Psi = \frac{1}{2} \mu_0 \Delta \chi (\mathbf{n} \cdot \mathbf{H})^2, \quad \mathbf{H} = H(\cos \phi_0, \sin \phi_0, 0), \quad \phi_0 = \text{constant}, \quad |\mathbf{H}| = H < \infty. \quad (14)$$

The related external generalised body force G_i is given by

$$G_i = \frac{\partial \Psi}{\partial n_i} = \mu_0 \Delta \chi (\mathbf{n} \cdot \mathbf{H}) H_i, \quad (15)$$

where $\mu_0 > 0$ is the permeability of free space and $\Delta \chi$ is a dimensionless measure of magnetic anisotropy. It will be assumed that $\Delta \chi > 0$ since this is valid for most nematics.

3.1 The non-dimensionalised dynamic equations

We consider Cartesian flows and employ the change of variables

$$x_i = L\hat{x}_i, u_i = U\hat{u}_i, t = LU^{-1}\hat{t}, p = \rho U^2\hat{p}, \tilde{t}_{ij} = \eta\hat{S}_{ij}, w_F = \rho U^2\hat{w}_F, \tilde{g}_j = \rho U^2\hat{R}_j, G_j = \rho U^2\hat{G}_j \quad (16)$$

where L, U and η denote ‘typical’ length, velocity and viscosity scales, respectively. This work used $\eta = \alpha_3 - \alpha_2$.

The incompressibility condition Eq. (1)₂, the elastic energy density Eq. (4) and the linear momentum equation Eq. (2) can then be expressed, respectively, in dimensionless form as

$$u_{i,i} = 0, \quad (17)$$

$$w_F = \frac{1}{2Re Er} \left[(\phi_{,x})^2 + (\phi_{,y})^2 \right] \quad (18)$$

$$\frac{\partial u_i}{\partial t} = -(\tilde{p} + \tilde{w}_F)_{,i} - (u_j u_i)_{,j} + R_j n_{j,i} + G_j n_{j,i} + \frac{1}{Re} (S_{ij,j}), \quad (19)$$

where $Re = \frac{\rho UL}{\eta}$ and $Er = UL \frac{\eta}{K}$ are the Reynolds and Ericksen numbers, respectively. For example, the terms $R_j n_{j,x}$ and $G_j n_{j,x}$ are given by

$$R_j n_{j,x} = \frac{1}{Re} \left\{ -\gamma_1 \phi_{,x} \left[\phi_{,t} + u\phi_{,x} + v\phi_{,y} + \frac{1}{2}(u_{,y} - v_{,x}) \right] - \frac{1}{2} \left[\gamma_2 \phi_{,x} \cos(2\phi)(u_{,y} + v_{,x}) + \gamma_2 \phi_{,x} \sin(2\phi)(u_{,x} - v_{,y}) \right] \right\}, \quad (20)$$

$$G_j n_{j,x} = \frac{1}{2} \mu_0 \Delta \chi H^2 \phi_{,x} \sin(2(\phi_0 - \phi)), \quad (21)$$

and the non-dimensional component S_{xx} of the extra-stress tensor is calculated to give

$$S_{xx} = \alpha_1 \cos^2 \phi \left[u_{,x} \cos^2 \phi + v_{,y} \sin^2 \phi + \frac{1}{2}(u_{,y} + v_{,x}) \sin(2\phi) \right] - (\alpha_2 + \alpha_3) \sin \phi \cos \phi \left[\phi_{,t} + u\phi_{,x} + v\phi_{,y} + \frac{1}{2}(u_{,y} - v_{,x}) \right] + \alpha_4 u_{,x} + (\alpha_5 + \alpha_6) \left[u_{,x} \cos^2 \phi + \frac{1}{2} \sin \phi \cos \phi (u_{,y} + v_{,x}) \right], \quad (22)$$

In the equations above, the viscosities $\alpha_1, \dots, \alpha_6$ have been scaled by a factor of η .

The angular momentum equation Eq. (3) becomes

$$\phi_{,t} + u\phi_{,x} + v\phi_{,y} = \frac{1}{Er \gamma_1} \left[\phi_{,xx} + \phi_{,yy} \right] - \frac{1}{2}(u_{,y} - v_{,x}) - \frac{1}{2} \frac{\gamma_2}{\gamma_1} \left[(u_{,y} + v_{,x}) \cos(2\phi) + (v_{,y} - u_{,x}) \sin(2\phi) \right] - \frac{1}{2} \frac{Re}{\gamma_1} \mu_0 \Delta \chi H^2 \sin(2(\phi_0 - \phi)). \quad (23)$$

In Eqs. (18)-(23) the circumflexes have been omitted for notational clarity.

Equations (17), (19) and Eq. (23) form the complete set of dynamic equations and must be solved subject to suitable boundary conditions in order to find solutions for ϕ, p and u_i .

4. NUMERICAL METHOD

In order to solve Eqs. (17), (19) and Eq. (23) we first write the components of the stress tensor S_{ij} in the following manner:

$$S_{ij} = \frac{1}{Re} \left[\alpha_4 (u_{i,j} + u_{j,i}) + \Phi_{ij} \right] \quad (24)$$

where Φ_{ij} is called the non-Newtonian stress tensor, hereafter, given by

$$\Phi_{ij} = \alpha_1 n_k A_{kp} n_p n_i n_j + \alpha_2 N_i n_j + \alpha_3 n_i N_j + \alpha_5 n_j A_{ik} n_k + \alpha_6 n_i A_{jk} n_k. \quad (25)$$

For example, the component Φ_{xx} of the non-Newtonian stress tensor is given by

$$\Phi_{xx} = \alpha_1 \cos^2 \phi \left[u_{,x} \cos^2 \phi + v_{,y} \sin^2 \phi + \frac{1}{2}(u_{,y} + v_{,x}) \sin(2\phi) \right] - (\alpha_2 + \alpha_3) \sin \phi \cos \phi \left[\phi_{,t} + u\phi_{,x} + v\phi_{,y} + \frac{1}{2}(u_{,y} - v_{,x}) \right] + (\alpha_5 + \alpha_6) \left[u_{,x} \cos^2 \phi + \frac{1}{2} \sin \phi \cos \phi (u_{,y} + v_{,x}) \right]. \quad (26)$$

Thus, the equation of motion Eq. (19) can be written in the form

$$\frac{\partial u_i}{\partial t} = -(p + w_F)_{,i} - (u_j u_i)_{,j} + R_j n_{j,i} + G_j n_{j,i} + \frac{1}{Re} ((u_{i,j})_{,j} + \Phi_{ij,j}). \quad (27)$$

4.1 Boundary conditions

In order to solve Eqs. (17), (27) and (23) it is necessary to impose boundary conditions for the velocity field on mesh boundaries. For rigid boundaries we employ the no-slip condition ($u_i = 0$) while at fluid entrances (inflows) the normal velocity is specified by $u_\nu = U_{inf}$ and the tangential velocities are set to zero, namely, $u_\mu = 0$, where ν denotes normal direction to the boundary and μ denotes tangential directions. At fluid exits (outflows) the Neumann condition $u_{i,\nu} = 0$ is adopted.

The director is strongly anchored on rigid boundaries (walls). In other words, the fixed director orientation angle is set according to the prescribed orientation of the rigid boundary. Details of this anchoring angle will be given in the section dealing with the numerical results.

The choice of the angle of the director at fluid entrances (inflows) is $\phi = 0$ and at fluid exits (outflows) we set $\phi_{,\nu} = 0$.

4.2 Procedure

The momentum equation Eq. (27), the mass conservation equation Eq. (17) and the angular momentum equation Eq. (23) will be solved by a methodology based on the GENSMAC algorithm introduced by Tomé et al. (2002) as follows.

Assume that, at time t_n , the velocity field $u_i(x_k, t_n)$ and the orientation angle of the director $\phi(x_k, t_n)$ are known and that suitable boundary conditions are provided. In order to calculate the velocity field $u_i(x_k, t_{n+1})$, the pressure $p(x_k, t_{n+1})$, the non-Newtonian tensor $\Phi_{ij}(x_k, t_{n+1})$ and the orientation angle of the director $\phi(x_k, t_{n+1})$ we proceed in the following manner:

Step 1: Using the values of $u_i(x_k, t_n)$ and $\phi(x_k, t_n)$, solve Eq. (18) for $w_F(x_k, t_n)$ and calculate $w_{F,i}(x_k, t_n)$, $\Phi_{ij}(x_k, t_n)$, $R_j n_{j,i}(x_k, t_n)$, $G_j n_{j,i}(x_k, t_n)$.

Step 2: Calculate the intermediate velocity field $\tilde{u}_i(x_k, t_{n+1})$ from

$$\frac{\partial \tilde{u}_i}{\partial t} = -(u_j u_i)_{,j} - \tilde{w}_{F,i} + R_j n_{j,i} + G_j n_{j,i} \frac{1}{Re} [(u_{i,j})_{,j} + \Phi_{ij,j}] \quad (28)$$

with $\tilde{u}_i(x_k, t_n) = u_i(x_k, t_n)$ using the same boundary conditions for the velocity $u_i(x_k, t_n)$. This equation is solved by an explicit finite difference method.

Step 3: Solve the Poisson equation

$$\psi_{,ii}(x_k, t_{n+1}) = \tilde{u}_{i,i}(x_k, t_{n+1}) \quad (29)$$

subject to the boundary conditions (see Tomé and McKee (1994)): $\psi_{,\nu} = 0$ on rigid boundary and inflows and $\psi = 0$ on outflows.

Step 4: Calculate the velocity field

$$u_i(x_k, t_{n+1}) = \tilde{u}_i(x_k, t_{n+1}) - \psi_{,i}(x_k, t_{n+1}) \quad (30)$$

Step 5: Determine the pressure field $p(x_k, t_{n+1})$ (see Tomé et al. (1996))

$$p(x_k, t_{n+1}) = \frac{\psi(x_k, t_{n+1})}{\delta t} \quad (31)$$

Step 6: Calculate the angle of the director $\phi(x_k, t_{n+1})$ from Eq. (23). This equation is solved by an explicit finite difference method.

Step 7: Calculate the components of the non-Newtonian tensor $\Phi_{ij}(x_k, t_{n+1})$ from equation Eq. (25).

5. FINITE DIFFERENCE APPROXIMATION

The equations contained in the procedure outlined in the previous section will be solved by the finite difference method as follows. A staggered grid is employed. The velocities u and v are located at the middle of cell faces while the other quantities (ϕ , Φ , p , w_F) are positioned at cell centres.

The momentum conservation equation Eq. (27) and the angular momentum equation Eq. (23) are solved by the explicit Euler method. The spatial derivatives in the momentum conservation equations are discretised at the points $((i + \frac{1}{2})\delta x, j\delta y)$ and $(i\delta x, (j + \frac{1}{2})\delta y)$ while the angular momentum equation Eq. (23), the density of elastic energy Eq. (18) and the tensor Φ_{ij} are approximated at cell centres $(i\delta x, j\delta y)$.

Terms involving the pressure gradient, the divergence of the non-Newtonian stress tensor, the gradient of the density of elastic energy, the external force and terms $R_j n_{j,x}$, $R_j n_{j,y}$ are approximated by central differences.

6. VALIDATION RESULTS

The equations in Sec. 4. were implemented into an existing computer code which was applied to simulate steady flow of a nematic liquid crystal MBBA at 25°C.

The numerical method was validated by simulating the flow of a nematic liquid crystal in a 2D-channel. We considered a channel with width L and length $C = 10L$. The boundary conditions for the velocity field were those specified in Sec. 4.1. At the fluid entrance, a fully developed flow given by

$$u(y) = -4\frac{U}{L}\left(y - \frac{L}{2}\right)^2 + U \quad (32)$$

was imposed.

To simulate this problem, the following input data specifying the flow were employed:

- Width of the entry of plane: $L = 0.001\text{m}$; Velocity scale: $U = 0.00038 \text{ ms}^{-1}$; angle of magnetic field: $\phi_0 = 0^\circ$.

The physical parameters, specifying the nematic liquid crystal MBBA at 25°C are given in Tables 1 and 2. With these data we obtain $Re = 0.039$ and $Er = 55.38$. To show the convergence of the numerical method presented in this paper, we simulated channel flow in four meshes until steady state was achieved. The meshes employed were: M_0 : $\delta x = \delta y = 0.000125\text{m}$ (80×8 cells); M_1 : $\delta x = \delta y = 0.0000625\text{m}$ (160×16 cells); M_2 : $\delta x = \delta y = 0.00003125\text{m}$ (320×32 cells) and M_3 : $\delta x = \delta y = 0.000015625\text{m}$ (640×64 cells). We are not aware of an analytic solution for this problem so that we compared the solutions obtained on meshes M_0 , M_1 and M_2 to the solution obtained on the finer mesh M_3 which we refer here as *EXACT*. Figure 1 displays the numerical and the *EXACT* values of $u(y)$, Φ_{xx} , Φ_{xy} and Φ_{yx} at the end of the channel ($x = 10$). We can see that there is good agreement between the solutions. Moreover, Figs. 1 and ?? show that as the mesh is refined the numerical solutions tend to the *EXACT* solution. These results show the convergence of the numerical method presented in this work.

Table 1. Leslie viscosities for the nematic liquid crystal at MBBA given in SI units (see Stewart (2004)).

Leslie viscosities	α_1	α_2	α_3	α_4	α_5	α_6
MBBA near 25°C	-0.0181	-0.1104	-0.001104	0.0826	0.0779	-0.0336

Table 2. Physical parameters for the nematic phases of MBBA given in SI units (see Stewart (2004)). The abbreviations used are: magnetic anisotropy ($\Delta\chi$ (unitless)) (see Stephen and Straley (1974)), density (ρ) (see Stephen and Straley (1974)), permeability of free space (μ_0), magnetic field (H) and elastic constant (K).

Physical parameters	$\Delta\chi$	ρ	μ_0	H	K
MBBA near 25°C	1.219×10^{-6}	1088 kg m^{-3}	$12.566 \times 10^{-7} \text{ H m}^{-1}$	$\frac{1}{4\pi} 10^3 \text{ A m}^{-1}$	$7.5 \times 10^{-10} \text{ N}$

7. NUMERICAL INVESTIGATION OF THE FLOW OF NEMATIC LIQUID CRYSTALS IN L-CHANNELS

We applied the technique presented in this work to simulate the flow of a nematic liquid crystals in a two-dimensional L-shaped channel (see Fig. 2). On the channel walls we set $u_i = 0$ and at the channel entrance the velocity was given by Eq. (32) presented in the previous section.

7.1 Boundary conditions for the angle ϕ

The boundary conditions for the angle ϕ were specified as follows:

1. Along the horizontal walls, the anchoring angle was set to zero, implying parallel alignment to the walls.
2. At the re-entrant corner, we used:
 - (a) $\phi = -45^\circ$ (see Fig. 2(a));
 - (b) $\phi = 0$ (see Fig. 2(b));
 - (c) $\phi = 45^\circ$ (see Fig. 2(c)).
3. At the vertical walls, we employed:
 - (a) $\phi = -90^\circ$ at $x = C$, $0 \leq y \leq H$ and $x = C - L1$, $0 \leq y \leq H - L$ (see Fig. 2(a));
 - (b) $\phi = 0$ at $x = C$, $0 \leq y \leq H$ and $x = C - L1$, $0 \leq y \leq H - L$ (see Fig. 2(b));
 - (c) $\phi = 90^\circ$ at $x = C$, $0 \leq y \leq H$ and $x = C - L1$, $0 \leq y \leq H - L$ (see Fig. 2(c)).
4. At the channel entry we set $\phi = 0$ and at the exit plane we assumed $\phi_{,y} = 0$.

The physical parameters specific to the nematic liquid crystal MBBA at 25°C employed to simulate this problem are presented in Tables 1 and 2.

The remaining parameters specifying the flow were:

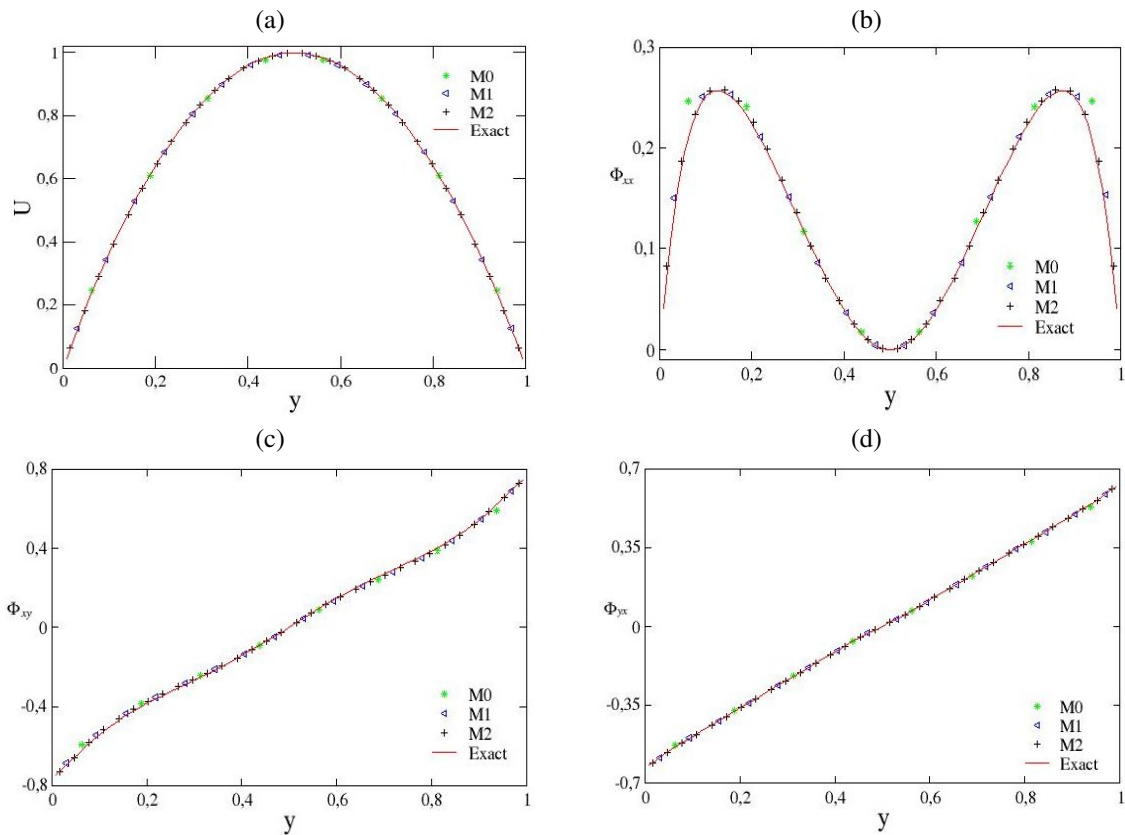


Figure 1. Comparison between the *EXACT* and the numerical solutions at $x = 10$. (a) Velocity field, (b) Φ_{xx} , (c) Φ_{xy} and (d) Φ_{yx} .

- Mesh (**M**): 60×60 cells ($\delta x = \delta y = 0.0001$)m; Width of the entry of plane: $L = 0.001$ m;
- Length of the horizontal channel: $C = 0.006$ m; Length of the vertical channel: $H = 0.006$ m;
- Velocity at inflow: $V_{inf} = 0.001 \text{ ms}^{-1}$; Velocity scale: $U = 0.001 \text{ ms}^{-1}$; angle of magnetic field: $\phi_0 = 0^\circ$;
- The width of the channel exit ($L1$) was varied so that this problem was simulated for the following ratios ($Ri = L1/L$): $R1 = 1$, $R2 = 0.5$ and $R3 = 0.3$;

The Reynolds number was calculated using the channel exit width $L1$ so that we had $Re = 0.005$ ($R1 = 1$), $Re = 0.0025$ ($R2 = 0.5$) and $Re = 0.0015$ ($R3 = 0.3$). In the results that follow the following Ericksen numbers ($Er = \frac{U L1 \eta}{K}$) were employed:

- for $Re = 0.005$,

$$Er = 7.2 \implies K = 7.5 \times 10^{-9}$$

- for $Re = 0.0025$,

$$Er = 36.4 \implies K = 7.5 \times 10^{-10}; \quad Er = 364.0 \implies K = 7.5 \times 10^{-11}; \quad Er = 3643.0 \implies K = 7.5 \times 10^{-12}.$$

- for $Re = 0.0015$,

$$Er = 21.8 \implies K = 7.5 \times 10^{-10}; \quad Er = 218.0 \implies K = 7.5 \times 10^{-11}; \quad Er = 2180.0 \implies K = 7.5 \times 10^{-12}.$$

To observe elastic and viscous effects in the flow, we simulated this problem for the values of Reynolds and Ericksen numbers given above until steady state was reached.

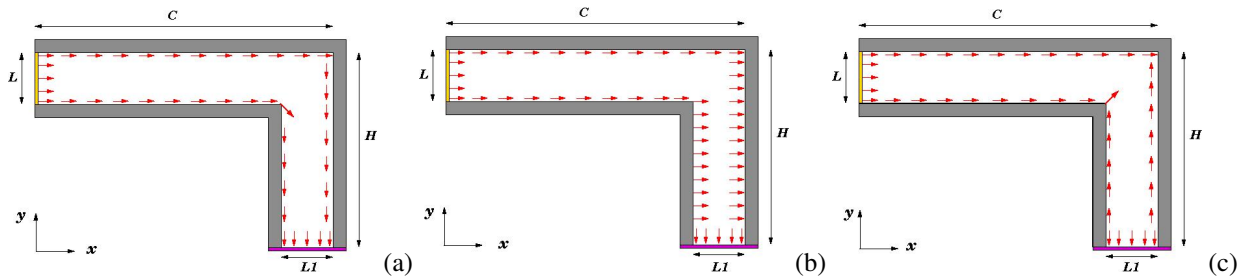


Figure 2. Definition of the domain for the simulation of the flow in a two-dimensional L-shaped channel. The red arrows represent the boundary conditions used for the calculation of the angle ϕ by means of Eq. (23).

Figure 3 displays the isolines of pressure and velocity at time $t = 24$ for the case $Re = 0.005$ and $Er = 7.2$ with the boundary conditions for the director displayed in Fig. 2(a). We can see in Fig. 3(a) that the isolines in the exit channel indicates that the pressure varies only in y -direction. However, the isolines in Fig. 3(b) show that the velocity u is zero in the downstream channel where, in Fig. 3(c), the isolines of velocity v are parallel. These results indicate that steady state has been reached. The same profiles were obtained for the other Reynolds and Ericksen numbers.

To demonstrate the effect of the boundary conditions on the director field, we performed three simulations using $Re = 0.005$ and $Er = 7.2$. In the first simulation we used the boundary conditions displayed in Fig. 2(a) while in the second and third simulations we employed the boundary conditions depicted in Fig. 2(b) and Fig. 2(c), respectively. Each of these simulations were performed until $t = 24$. A zoom-up of the solutions obtained for the director near the re-entrant corner of the L-shaped channel are shown in Fig. 4 while Fig. 7 displays the streamlines of the velocity in the entire L-shaped channel. We can observe in Fig. 4 that the effect of the boundary conditions upon the angle ϕ is very interesting. In the first simulation (see Fig. 4(a)) the director profile did not display large variations: the orientation of the director is mostly uniform throughout the L-shaped channel. In the second simulation (see Fig. 4(b)) we can see that the director in the downstream channel was strongly affected by the boundary conditions which forced the director to be at 0° (perpendicular to the downstream walls). Similarly, in the third simulation, when the angle ϕ along the downstream walls was set opposite to the main flow direction (90°), the director was again strongly affected by the boundary conditions making it to lie at 90° along the downstream walls (see Fig. 4(c)). On the other hand, Fig. 7 shows that the different boundary conditions applied to the director did not impose major changes in the streamlines of the velocity in the L-shaped channel: the streamlines are smooth along the L-shaped channel. Such behavior was similar to that observed in certain viscoelastic fluids (see Chono and Iemoto (1992)).

In order to investigate the effect of Er and the ratio $Ri = L1/L$ on the flow, we performed three simulations using $Re = 0.0025$ ($R2 = 0.5$) and $Er = 36.4, 364.0, 3643.0$. It is known that Er is typically $10^4 Re$ for many nematics (see Stewart (2004)). The boundary conditions used were those displayed in Fig. 2(a). A zoom-up of the solutions obtained for the director near the re-entrant corner of the L-shaped channel is shown in Fig. 5 while Fig. 8 displays the streamlines of the velocity in the L-shaped channel. We can observe in Fig. 5(a) that for $Er = 36.4$ the director accommodates the boundary conditions and converges to the centerline of the channels. The results obtained for $Er = 364.0$ (see Fig. 5(b)) were similar to the case $Er = 36.4$ except for the vectors adjacent to the left wall of the downstream channel where we can see that the director did not obey the imposed boundary condition of -90° . As the Ericksen number is increased to 3643.0, Fig. 5(c) shows that the director profile became very complex in the re-entrant channel. Rotation of the director made it pointing vertically upwards. The corresponding streamlines displayed in Fig. 8 are very interesting as we see a lip vortex for $Er = 36.4$ (see Fig. 8(a)) which decreases at $Er = 364.0$ (see Fig. 8(b)) and almost vanishes when $Er = 3643.0$ (see Fig. 8(c)). We believe that the appearance of the lip vortex was due to the change in the geometry because in the results obtained for $Er = 7.2$ (see Fig. 7(a)) a lip vortex was not present. To confirm this fact, we performed three more simulations for $Re = 0.0015$ ($R3 = 0.3$) and $Er = 21.8, 218.0, 2180.0$ using the boundary conditions displayed in Fig. 2(a). The director profiles obtained in these simulations are shown in Fig. 6 while the streamlines are displayed in Fig. 9. We can see that the director profiles are similar to those obtained for $Re = 0.0025$ (see Fig. 5). However, as we can see from Fig. 9, the effect of the change in geometry caused the appearance of a larger lip vortex which decreased very little when the Ericksen number was increased. A similar result was obtained by Chono and Iemoto (1992) using the White Metzner model to simulate the flow of a polyacrylamid solution in a L-shaped channel.

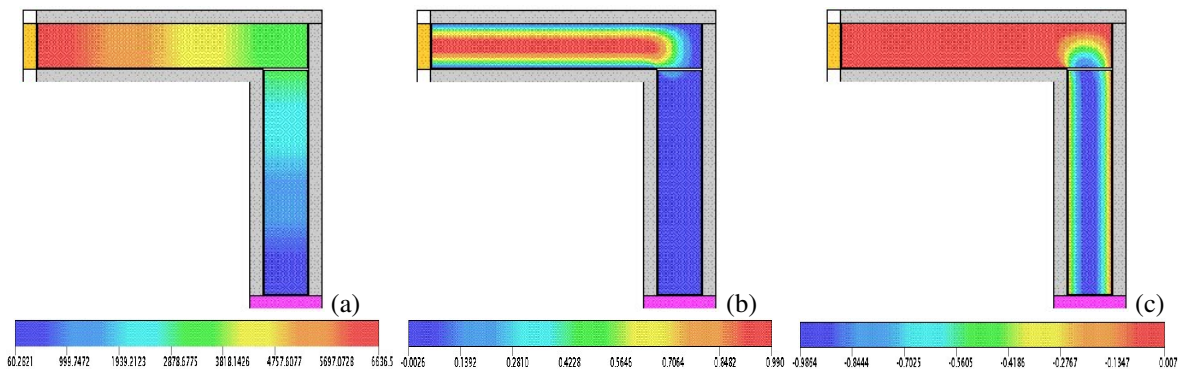


Figure 3. Numerical simulation of the flow through a L-shaped channel with $Re = 0.005$ and $Er = 7.2$. Isolines: (a) Pressure, (b) Velocity u and (c) Velocity v .

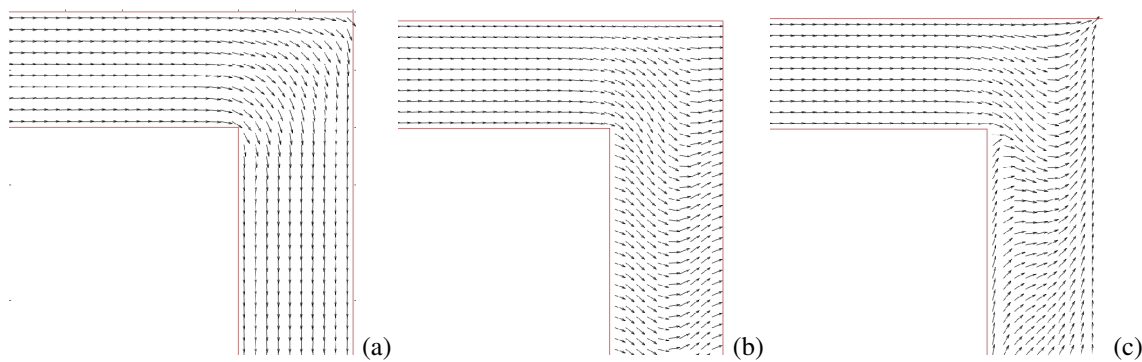


Figure 4. Numerical simulation of the director through a L-shaped channel with $Re = 0.005$ and $Er = 7.2$. Plots of director for different boundary conditions for the angle ϕ : (a) $\phi = -90^\circ$, (b) $\phi = 0$, and (c) $\phi = 90^\circ$.

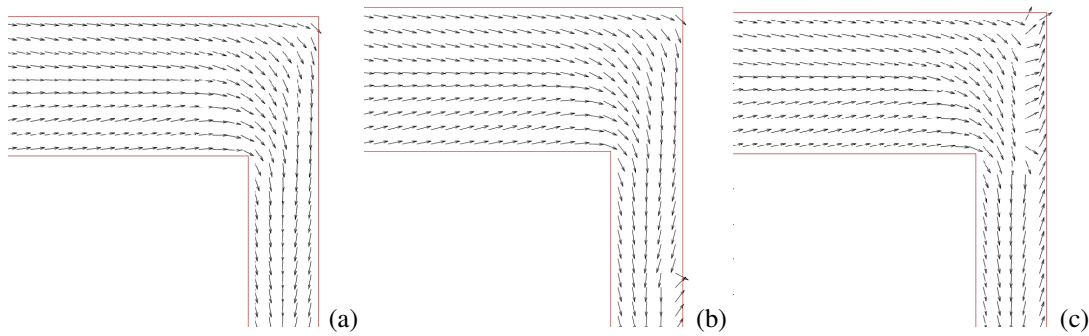


Figure 5. Numerical simulation of the director through a L-shaped channel with $Re = 0.0025$. Plots of director for different Ericksen numbers: (a) $Er = 36.4$, (b) $Er = 364.0$ and (c) $Er = 3643.0$.

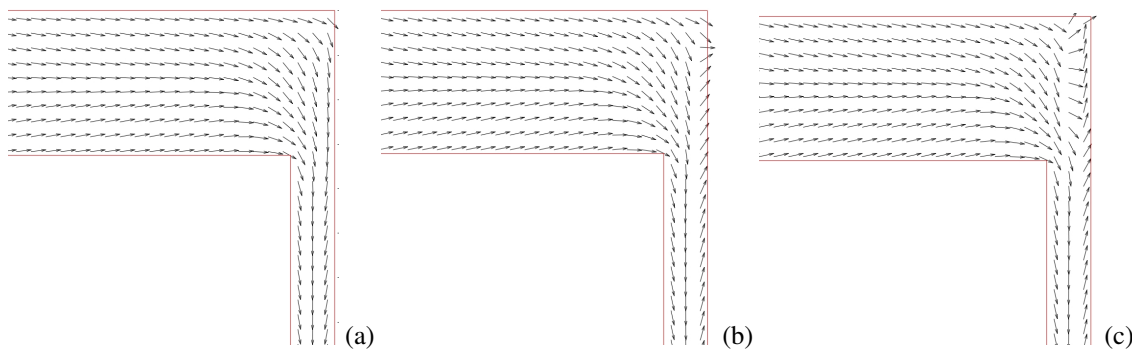


Figure 6. Numerical simulation of the director through a L-shaped channel with $Re = 0.0015$. Plots of the director for different Ericksen numbers: (a) $Er = 21.8$, (b) $Er = 218.0$ and (c) $Er = 2180.0$.

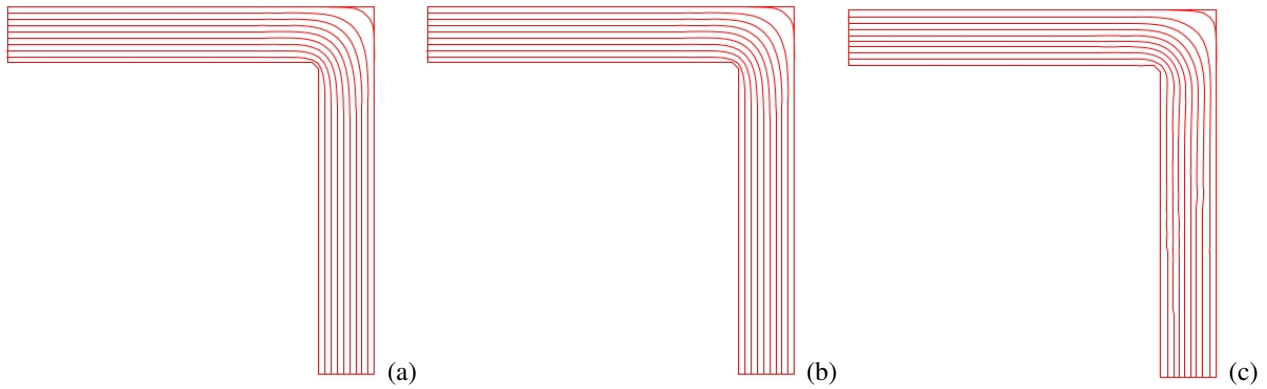


Figure 7. Plots of streamlines for $Re = 0.005$ and $Er = 7.2$: (a) ($\phi = -90^\circ$), (b) ($\phi = 0$) and (c) ($\phi = 90^\circ$).

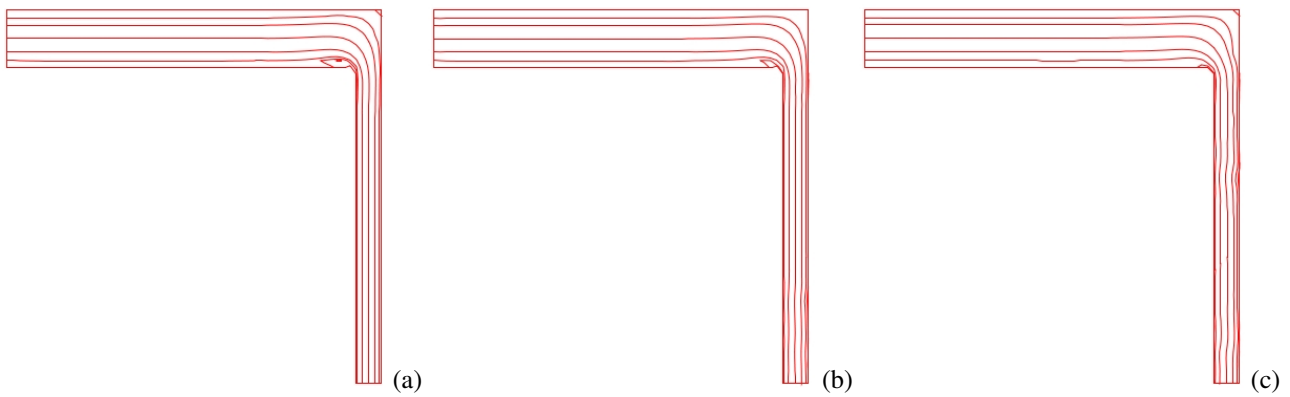


Figure 8. Plots of streamlines for $Re = 0.0025$ and different Ericksen numbers: (a) $Er = 36.4$, (b) $Er = 364.0$ and (c) $Er = 3643.0$.

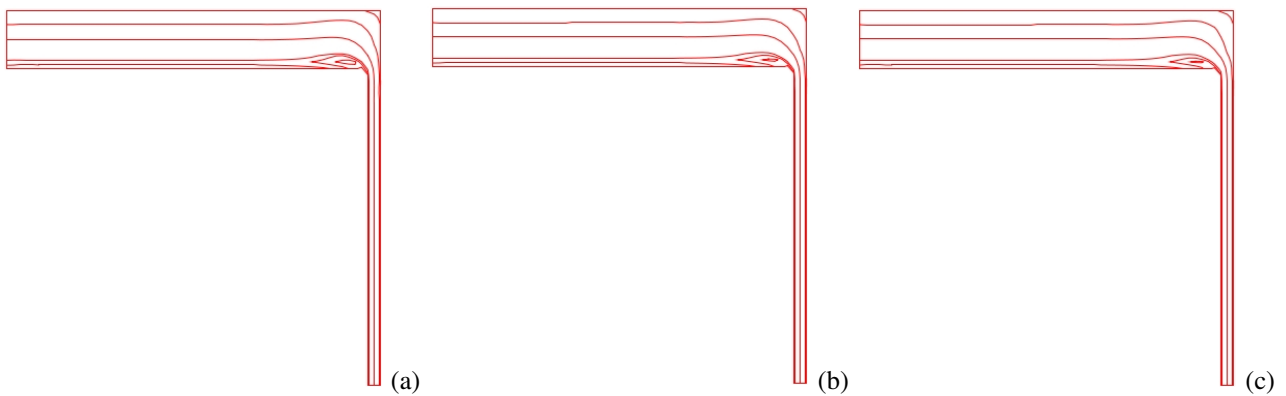


Figure 9. Plots of streamlines for $Re = 0.0015$ and different Ericksen numbers: (a) $Er = 21.8$, (b) $Er = 218.0$ and (c) $Er = 2180.0$.

8. CONCLUSIONS

This paper dealt with the development of a numerical method for solving two-dimensional flows of nematic liquid crystals subject to a finite magnetic field. The numerical technique developed herein was based on the finite difference method developed by Tomé et al. (2002). The validation of the technique was performed through the simulation of the flow in a channel using four meshes: M0, M1, M2 and M3. An analytic solution for this problem is not yet available, so we compared the solutions on meshes M0, M1 and M2 to the solution obtained on the finer mesh M3 (which we called *EXACT*). Good agreement between the solutions obtained on the coarser meshes and the solution on mesh M3 was observed. Moreover, the flow in a L-shaped channel was simulated for various values of the Reynolds and Ericksen numbers and interesting effects were obtained. The results showed that when the ratio of the width of the exit channel to width of the entrance channel ($Ri = L1/L$) was decreased this caused the appearance of a lip vortex at the re-entrant channel. It was shown that this lip vortex can disappear (in the case high Ericksen number) or become larger (as the ratio is decreased).

9. ACKNOWLEDGEMENTS

The authors would like to acknowledge the financial support given by the Brazilian funding agencies: FAPESP - Fundação de Amparo a pesquisa do Estado de São Paulo (grants 04/16064-9, 07/07038-2) and CNPq - Conselho Nacional de Desenvolvimento Científico e Tecnológico (grants Nos. 304422/2007-0, 470764/2007-4).

10. REFERENCES

- Baleo, J. N., Vincent, M. and Navard, P., 1998, Finite element simulation of flow and director orientation of viscous anisotropic fluids in complex 2D geometries. *Mol. Liq. Cryst.*, **309**, 217-236 .
- Chono, S. and Iemoto, Y., 1992, Numerical simulation of viscoelastic flow in two-dimensional L-shaped channels, *J. Rheol.*, **36**, 335-356 .
- Chono, S. and Tsuji, T., 1998, Numerical simulation of nematic liquid crystalline flows around a circular cylinder. *Mol. Liq. Cryst.*, **309**, 217-236 .
- Chono, S., Tsuji, T. and Denn, M. M., 1998, Spatial development of director orientation of tumbling nematic liquid crystals in pressure-driven channel flow. *J. Non-Newtonian Fluid Mech.*, **79**, 515-527 .
- Ericksen, J.L., 1961, Conservation laws for liquid crystals, *Trans. Soc. Rheol.*, **5**, 23-24 .
- Heuer, H., Kneppel, H. and Schneider, F., 1991, Flow of a Nematic Liquid Crystal Around a Cylinder, *Mol. Cryst. Liq. Cryst.*, **200**, 51-70 .
- Jenkins, J. T., 1978, Flows of Nematic Liquid Crystals, *Ann. Rev. Fluid Mech.*, **10**, 197-219 .
- Kneppel, H., Schneider, F. and Sharma, N.K., 1982, Rotational viscosity γ_1 of nematic liquid crystals, *J. Chem. Phys.*, **77**, 3203-3208 .
- Leslie, F.M., 1966, Some Constitutive Equations for Anisotropic Fluids, *Q. Jl. Mech. Appl. Math.*, **19**, 357-370 .
- Leslie, F.M., 1968, Some Constitutive Equations for Liquid Crystals, *Arch. Rat. Mech. Anal.*, **28**, 265-283 .
- MacSithigh, G. P. and Currie, P. K., 1977, Apparent viscosity during simple shearing flow of nematic liquid crystals. *J. Phys. D.*, **10**, 1471-1478 .
- Parodi, O., 1970, Stress Tensor for a Nematic Liquid Crystal, *J. de Physique*, **31**, 581-584 .
- Pieranski, P. and Guyon, E., 1974, Transverse Effects in Nematic Flows, *Physics Letters*, **49A**, 237-238 .
- Pikin, S. A., 1974, Couette flow of nematic liquid, *Sov. Phys. JETP*, **38A**, 1246 .
- Stephen, M.J. and Straley, J.P., 1974, Physics of Liquid Crystals, *Reviews of Modern Physics*, **46**, 617-704 .
- Stewart, I.W., 2004, The Static and Dynamic Continuum Theory of Liquid Crystals, Taylor and Francis, London.
- Tomé, M.F., Duffy, B. and McKee, S., 1996, A Numerical Technique for Solving Unsteady Non-Newtonian Free Surface Flows, *J. Non-Newtonian Fluid Mech.*, **62**, 9-34.
- Tomé, M.F., Mangiavacchi, N., Cuminato, J.A., Castelo, A. and McKee, S., 2002, A finite difference technique for simulating unsteady viscoelastic free surface flows, *J. Non-Newtonian Fluid Mech.*, **106**, 61-106 .
- Tomé, M. F. and McKee, S., (1994), GENSMAC: A computational marker-and-cell method for free surface flows in general domains, *Journal of Computational Physics*, **110**, 171-186.